Available online at www.sciencedirect.com

ScienceDirect

Procedia Structural Integrity 2 (2016) 1920–1927

Structural Integrity Procedia

www.elsevier.com/locate/procedia

21st European Conference on Fracture, ECF21, 20-24 June 2016, Catania, Italy

Reconstruction of a 2D stress field around the tip of a sharp material inclusion

Ondřej Krepl[a]*, Jan Klusák[a]

[a]*CEITEC IPM, Institute of Physics of Materials AS CR, Zizkova 22, Brno 616 62, Czech Republic*

Abstract

The stress distribution in the vicinity of a sharp material inclusion (SMI) tip exhibits a singular stress behavior. The strength of the stress singularity depends on material properties and geometry. The SMI is a special case of a general singular stress concentrator (GSSC). The stress field near a GSSC can be analytically described by means of Muskhelishvili plane elasticity based on complex variable function methods. Parameters necessary for the description are the exponents of singularity and generalized stress intensity factors (GSIFs). The stress field in the closest vicinity of an SMI tip is thus characterized by 1 or 2 singular exponents (λ-1), for which $0<Re(\lambda)<1$, and corresponding GSIFs. In order to describe a stress field further away from an SMI tip, the non-singular exponents, $1<Re(\lambda)$, and factors corresponding to these non-singular exponents have to be taken into account. For given boundary conditions of the SMI, the exponents are calculated as an eigenvalue problem. Then, by formation of corresponding eigenvectors, the stress or displacement angular functions for each stress or displacement series term are constructed. The contribution of each stress or displacement series term function to the total stress and displacement field is given by the corresponding GSIF. The GSIFs are calculated by the over deterministic method (ODM), which finds a solution of an over-determined system of linear equations by the least squares method. On the left-hand side of the system are the displacement series term functions multiplied by unknown GSIFs, while the right-hand is formed by results of finite element analysis (FEA). Thus the results of FEA, namely nodal displacements in the radial and tangential direction, are employed in order to obtain the GSIFs. In the numerical example, the stress field for particular bi-material configurations and geometries is reconstructed using i) singular terms only ii) singular and non-singular terms. The reconstructed stress field polar plots are compared with FEA results.

Peer-review under responsibility of the Scientific Committee of ECF21.

Keywords: Generalized Fracture Mechanics, General Singular Stress Concentrator, Sharp Material Inclusion, Muskhelishvili plane elasticity

* Corresponding author. Tel.: +420 532 290 338
E-mail address: krepl@ipm.cz

Copyright © 2016 The Authors. Published by Elsevier B.V. This is an open access article under the CC BY-NC-ND license (http://creativecommons.org/licenses/by-nc-nd/4.0/).
Peer review under responsibility of the Scientific Committee of ECF21.
10.1016/j.prostr.2016.06.241

1. Introduction

Composite materials which consist of two or more components with different material properties are often encountered in various engineering applications. Silicate-based composites for instance, particularly cement-based composites, are usually composed of a silicate/cement paste matrix and mainly sandstone, granite or basalt aggregate. An important task in a material design process of a composite is the prediction of its strength and fracture toughness. Precise knowledge of the composite strength and its fracture parameters can also contribute to prevention of structure failure. It is the very nature of composites what brings a higher complexity into the modeling of fracture mechanisms. Obviously, the material parameters, namely the Young's moduli and Poisson's ratios of aggregate and a matrix, vary, therefore, there exists a mismatch in material properties. The mismatch in material properties together with the topology of aggregate, which can be regarded as material inclusions, is responsible for occurrence of singular stress concentration points. Therefore, one has to deal with a more difficult description of composites in terms of the elasticity theory and fracture mechanics. In general, the topology of silicate-based composite aggregate particles consists of sharp corners, which can be geometrically characterized by its angle value. The topology of aggregate consists of corners with either convex or concave angles. These sharp corners are points of singular stress concentration and thus suspicious as crack initiation locations. By application of the appropriate fracture criterion to these singular stress concentration points, micro-crack initiation in certain composite can be predicted. Precise description of the stress distribution in the vicinity of these general singular stress concentrators is therefore essential for an employment of such fracture criterion. Since the strength of the elastic stress singularity of these points is dependent on bi-material properties and geometry, by optimization of these, composites with enhanced fracture parameters on a macro scale can be designed. In addition, the understanding of micro-crack formation in the vicinity of sharp material inclusion tips may lead to better understanding of the silicate-based composite non-linear behavior.

Nomenclature

$\mathbf{A}$	matrix based on boundary conditions of the problem
α	opening angle describing the geometry of a sharp material inclusion
$f_{ijkm}(\theta)$, $f_{ikm}(\theta)$	angular functions for stress and displacement asymptotic series
H_k	generalized stress intensity factor
γ_0, γ_1	angles denoting the location of the 0th and the 1st material interface
Γ_0, Γ_1	denotes the 0th and the 1st interface
$\mathbf{M}^m{}_\theta$	elementary matrix
M_{km}, N_{km}, I_{km}, L_{km}	complex constants for the mth material and kth eigenvalue
λ_k	kth eigenvalue
σ_{rr}, $\sigma_{\theta\theta}$, $\tau_{r\theta}$	radial, tangential and shear stress components respectively
Ω^m	mth material region
Ω_{km}, ω_{km}	complex potential functions for the mth material and kth eigenvalue
u_r, u_θ	radial and tangential displacement components respectively
v_{km}	eigenvector of complex constants for for the kth eigenvalue and mth material
v_k	combined eigenvector of complex constants for for the kth eigenvalue and both material regions

2. The stress and displacement distribution in the vicinity of a sharp material inclusion tip

2.1. Boundary conditions of the problem

A sharp material inclusion is depicted in Fig. 1. Material regions which are characterized by elastic parameters are denoted by Ω^0 and Ω^1. The sharp material inclusion is characterized by its opening angle α. Perfect bonding at both the interfaces Γ_1 and Γ_0 is assumed.

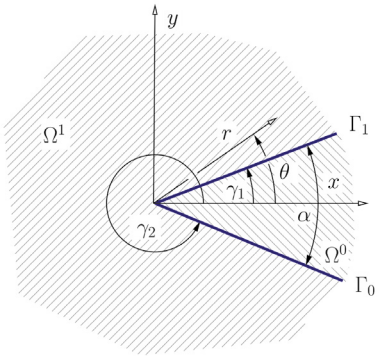

Fig. 1. A sharp material inclusion scheme.

Therefore, the boundary conditions represent stress and displacement continuity along the interfaces Γ_1 and Γ_0. The polar coordinate system as shown in Fig. 1 is considered. For the interface Γ_1 the boundary conditions are:

$$\begin{aligned} \sigma_\theta^0(r,\gamma_1) &= \sigma_\theta^1(r,\gamma_1) \\ \tau_{r\theta}^0(r,\gamma_1) &= \tau_{r\theta}^1(r,\gamma_1) \\ u_r^0(r,\gamma_1) &= u_r^1(r,\gamma_1) \\ u_\theta^0(r,\gamma_1) &= u_\theta^1(r,\gamma_1) \end{aligned} \tag{1}$$

in which the superscripts denote the corresponding material region. Note that the angle $\gamma_1 = \alpha/2$ applies in the equations for both the 0th and 1st material regions. The boundary conditions of the interface Γ_0 are given by the following equations:

$$\begin{aligned} \sigma_\theta^1(r,\gamma_2) &= \sigma_\theta^0(r,\gamma_0) \\ \tau_{r\theta}^1(r,\gamma_2) &= \tau_{r\theta}^0(r,\gamma_0) \\ u_r^1(r,\gamma_2) &= u_r^0(r,\gamma_0) \\ u_\theta^1(r,\gamma_2) &= u_\theta^0(r,\gamma_0) \end{aligned} \tag{2}$$

For the interface Γ_0 and the 0th material region the value of γ_0 is defined as $\gamma_0 = -\alpha/2$. For the 1st material region the value of γ_2 is given as $\gamma_2 = 2\pi - \alpha/2$.

2.2. Stress field in the vicinity of a general singular stress concentrator

The general expression describing the stress field in the vicinity of a singular point, i.e. when $r \to 0$, is given by asymptotic expansion

$$\sigma_{ij} = H_1 r^{\lambda_1 - 1} f_{ij1m}(\theta) + H_2 r^{\lambda_2 - 1} f_{ij2m} + H_3 r^{\lambda_3 - 1} f_{ij3m}(\theta) + \dots \tag{3}$$

where the exponent $(\lambda_k - 1)$ consists of the *k*th eigenvalue calculated as the solution of an eigenvalue problem of given boundary conditions. In general, complex eigenvalues are considered, $\lambda_k \in \mathbb{C}$. There are 1 or 2 eignevalues λ_k with their real part satisfying the relation $0 < \Re(\lambda_k) < 1$. The terms of the series which contain these 1 or 2 exponents become unbounded as $r \to 0$. Therefore, these are called exponents of singularity. Exponents with eigenvalues which real parts satisfy the relation $1 < \Re(\lambda_k)$ are also to be found, the terms which contain these exponents vanish as $r \to 0$, thus these exponents are called non-singular. The terms of the series with non-singular exponents describe a stress field further away from the singular point. The symbol H_k stands for the Generalized Stress Intensity Factor (GSIF). The symbol $f_{ijkm}(\theta)$ denotes angular functions where the indices *ij* denote corresponding stress tensor components, *k* refers to the *k*th eigenvalue and *m* to the *m*th material region. The series above applies for terms with real eigenvalues, its complex form is $\sigma_{ij} = \sum_{k=1}^{\infty} \frac{H_k}{2}\left[r^{\lambda_k - 1} f_{ijkm}(\theta) + r^{\bar{\lambda}_k - 1} \bar{f}_{ijkm}(\theta)\right]$.

There exist three different methods addressing the analysis of stress singularities in bonded homogenous media, namely the eigenvalue expansion method, the complex function representation and the Mellin transform technique. The application of the eigenvalue expansion method has been studied by Williams (1957) on crack problems and on reentrant corners in plates in extension in Williams (1957). Some problems with the Mellin transform technique applied can be found in Hein (1971) and Pageau et al. (1994). All three approaches are summarized in Paggi and Carpinteri (2008). Problems of bonded multi-material junction, which is the most general model of a sharp material inclusion, were addressed e.g. in Yang and Munz (1995), Sator and Becker (2011). This article deals with the complex function representation method. The mathematical theory of plane elasticity to address such configurations was developed by Muskhelishvili (1953) and England (2003). Muskhelishvili's approach is based on the complex variable function methods. The equations for stresses and displacements in the *m*th material can be written as:

$$\begin{aligned} \sigma_{rr}^{m} + i\tau_{r\theta}^{m} &= \Omega_m' + \bar{\Omega}_m' - z\bar{\Omega}_m'' - \frac{\bar{z}}{z}\bar{\omega}_m' \\ \sigma_{\theta\theta}^{m} - i\tau_{r\theta}^{m} &= \Omega_m' + \bar{\Omega}_m' + z\bar{\Omega}_m'' + \frac{\bar{z}}{z}\bar{\omega}_m' \\ u_r^m + iu_\theta^m &= \frac{1}{2G_m} e^{-i\theta}\left[\kappa_m\Omega_m - z\bar{\Omega}_m' - \bar{\omega}_m\right] \end{aligned} \tag{4}$$

where $z = re^{i\theta}$ is a complex variable in a polar coordinate system. The bar over the symbol (¯) denotes a complex conjugate and the symbol (') represents the derivative with respect to z. G_m is the shear modulus of the *m*th material and κ_m is the Kolosov constant of the *m*th material, which is given by the following relation:

$$\kappa_m = \begin{cases} 3 - 4\nu_m & \text{plane strain} \\ \frac{3-\nu_m}{1+\nu_m} & \text{plane stress} \end{cases} \tag{5}$$

in which ν_m is Poisson's ratio of the *m*th material. The stress and displacement components can be easily derived from (4) by adding a complex conjugate to both sides of a particular equation. Thus, the equations for stress and displacement components can be rewritten as:

$$\begin{aligned} \sigma_{rr}^{km} &= \Omega_{km}' + \bar{\Omega}_{km}' - \frac{\bar{z}}{2}\Omega_{km}'' - \frac{z}{2}\bar{\Omega}_{km}'' - \frac{z}{2\bar{z}}\omega_{km}' - \frac{\bar{z}}{2z}\bar{\omega}_{km}' \\ \sigma_{\theta\theta}^{km} &= \Omega_{km}' + \bar{\Omega}_{km}' + \frac{\bar{z}}{2}\Omega_{km}'' + \frac{z}{2}\bar{\Omega}_{km}'' + \frac{z}{2\bar{z}}\omega_{km}' + \frac{\bar{z}}{2z}\bar{\omega}_{km}' \\ \tau_{r\theta}^{km} &= \frac{\bar{z}}{2i}\Omega_{km}'' - \frac{z}{2i}\bar{\Omega}_{km}'' + \frac{z}{2i\bar{z}}\omega_{km}' - \frac{\bar{z}}{2iz}\bar{\omega}_{km}' \\ u_r^{km} &= \frac{1}{4G_i}\left\{e^{-i\theta}\left[\kappa_m\Omega_{km} - z\bar{\Omega}_{km} - \bar{\omega}_{km}\right] + e^{i\theta}\left[\kappa_m\bar{\Omega}_{km} - \bar{z}\Omega_{km} - \omega_{km}\right]\right\} \\ u_\theta^{km} &= \frac{1}{4iG_i}\left\{e^{-i\theta}\left[\kappa_m\Omega_{km} - z\bar{\Omega}_{km} - \bar{\omega}_{km}\right] - e^{i\theta}\left[\kappa_m\bar{\Omega}_{km} - \bar{z}\Omega_{km} - \omega_{km}\right]\right\} \end{aligned} \tag{6}$$

According to Theocaris (1974), the complex potentials Ω_{km} and ω_{km} can be constructed in the form of

$$\begin{aligned} \Omega_{km} &= I_{km}z^k + L_{km}z^{\bar{\lambda}_k} \\ \omega_{km} &= M_{km}z^{\lambda_k} + N_{km}z^{\bar{\lambda}_k} \end{aligned} \tag{7}$$

where I_{km}, L_{km}, M_{km} and N_{km} are unknown constants for the *m*th material and the *k*th eigenvalue λ_k. These constants or their complex conjugate form the *k*th eigenvector $v_{km} = (M_{km}, \bar{N}_{km}, I_{km}, \bar{L}_{km})$ for the *m*th material.

2.3. Determination of singular and non-singular exponents and corresponding eigenvectors

By introducing the potentials (7) into the equations for stress and displacement components (6) and by doing basic algebraic operations, we obtain a set of the following equations (8) - (12). Each of the equations is considered with unit GSIF $H_k = 1$. Based on the boundary conditions for both interfaces Γ_1 and Γ_0, (1) and (2) respectively, a system of 8 equations for stress and displacement components is formed. The system of equations arisen for our problem contains 9 unknowns. These are 4 complex constants I_{km}, L_{km}, M_{km} and N_{km} in each of the 2 eigenvectors v_{k0}, v_{k1} and the eigenvalue λ_k. The eigenvectors form one vector v_k in the following form $v_k = (v_{k0}, v_{k1})^T$.

$$\begin{aligned}\sigma_{rr}^{km} &= \frac{1}{2}\{r^{\lambda_k-1}\left[-I_{km}\lambda_k\left(\lambda_k-3\right)e^{i\theta(\lambda_k-1)}-\bar{L}_{km}\lambda_k\left(\lambda_k-3\right)e^{-i\theta(\lambda_k-1)}-M_{km}\lambda_k e^{i\theta(\lambda_k+1)}-\bar{N}_{km}\lambda_k e^{-i\theta(\lambda_k+1)}\right]+\\ &+ r^{\bar{\lambda}_k-1}\left[-\bar{I}_{km}\bar{\lambda}_k\left(\bar{\lambda}_k-3\right)e^{-i\theta\left(\bar{\lambda}_k-1\right)}-L_{km}\bar{\lambda}_k\left(\bar{\lambda}_k-3\right)e^{i\theta\left(\bar{\lambda}_k-1\right)}-\bar{M}_{km}\bar{\lambda}_k e^{-i\theta\left(\bar{\lambda}_k+1\right)}-N_{km}\bar{\lambda}_k e^{i\theta(\lambda_k+1)}\right]\}\end{aligned} \tag{8}$$

$$\begin{aligned}\sigma_{\theta\theta}^{km} &= \frac{1}{2}\{r^{\lambda_k-1}\left[I_{km}\lambda_k\left(\lambda_k+1\right)e^{i\theta(\lambda_k-1)}+\bar{L}_{km}\lambda_k\left(\lambda_k+1\right)e^{-i\theta(\lambda_k-1)}+M_{km}\lambda_k e^{i\theta(\lambda_k+1)}+\bar{N}_{km}\lambda_k e^{-i\theta(\lambda_k+1)}\right]+\\ &+ r^{\bar{\lambda}_k-1}\left[\bar{I}_{km}\bar{\lambda}_k\left(\bar{\lambda}_k+1\right)e^{-i\theta\left(\bar{\lambda}_k-1\right)}+L_{km}\bar{\lambda}_k\left(\bar{\lambda}_k+1\right)e^{i\theta\left(\bar{\lambda}_k-1\right)}+\bar{M}_{km}\bar{\lambda}_k e^{-i\theta\left(\bar{\lambda}_k+1\right)}+N_{km}\bar{\lambda}_k e^{i\theta(\lambda_k+1)}\right]\}\end{aligned} \tag{9}$$

$$\begin{aligned}\tau_{r\theta}^{km} &= \frac{1}{2i}\{r^{\lambda_k-1}\left[I_{km}\lambda_k\left(\lambda_k-1\right)e^{i\theta(\lambda_k-1)}-\bar{L}_{km}\lambda_k\left(\lambda_k-1\right)e^{-i\theta(\lambda_k-1)}+M_{km}\lambda_k e^{i\theta(\lambda_k+1)}-\bar{N}_{km}\lambda_k e^{-i\theta(\lambda_k+1)}\right]+\\ &+ r^{\bar{\lambda}_k-1}\left[-\bar{I}_{km}\bar{\lambda}_k\left(\bar{\lambda}_k-1\right)e^{-i\theta\left(\bar{\lambda}_k-1\right)}+L_{km}\bar{\lambda}_k\left(\bar{\lambda}_k-1\right)e^{i\theta\left(\bar{\lambda}_k-1\right)}-\bar{M}_{km}\bar{\lambda}_k e^{-i\theta\left(\bar{\lambda}_k+1\right)}+N_{km}\bar{\lambda}_k e^{i\theta\left(\bar{\lambda}_k+1\right)}\right]\}\end{aligned} \tag{10}$$

$$\begin{aligned}u_r^{km} &= \frac{1}{4G_m}\{r^{\lambda_k}\left[I_{km}\left(\kappa_m-\lambda_k\right)e^{i\theta(\lambda_k-1)}+\bar{L}_{km}\left(\kappa_m-\lambda_k\right)e^{-i\theta(\lambda_k-1)}-M_{km}e^{i\theta(\lambda_k+1)}-\bar{N}_{km}e^{-i\theta(\lambda_k+1)}\right]+\\ &+ r^{\bar{\lambda}_k}\left[\bar{I}_{km}\left(\kappa_m-\bar{\lambda}_k\right)e^{-i\theta\left(\bar{\lambda}_k-1\right)}+L_{km}\left(\kappa_m-\lambda_k\right)e^{i\theta(\lambda_k-1)}-\bar{M}_{km}e^{-i\theta(\lambda_k+1)}-N_{km}e^{i\theta(\lambda_k+1)}\right]\}\end{aligned} \tag{11}$$

$$\begin{aligned}u_\theta^{km} &= \frac{1}{4iG_m}\{r^{\lambda_k}\left[I_{km}\left(\kappa_m+\lambda_k\right)e^{i\theta(\lambda_k-1)}-\bar{L}_{km}\left(\kappa_m+\lambda_k\right)e^{-i\theta(\lambda_k-1)}+M_{km}e^{i\theta(\lambda_k+1)}-\bar{N}_{km}e^{-i\theta(\lambda_k+1)}\right]+\\ &+ r^{\bar{\lambda}_k}\left[-\bar{I}_{km}\left(\kappa_m+\bar{\lambda}_k\right)e^{-i\theta\left(\bar{\lambda}_k-1\right)}+L_{km}\left(\kappa_m+\bar{\lambda}_k\right)e^{i\theta\left(\bar{\lambda}_k-1\right)}-\bar{M}_{km}e^{-i\theta\left(\bar{\lambda}_k+1\right)}+N_{km}e^{i\theta\left(\bar{\lambda}_k+1\right)}\right]\}\end{aligned} \tag{12}$$

By simple algebraic operations, this system of 8 equations can be rearranged and symbolically written as:

$$\mathbf{A}v = 0 \tag{13}$$

The subscript for the eigenvector is intentionally omitted. Probably the most convenient way to construct a system of equations for any multi-material junction without a need for rearrangement described above is to form a matrix **A** from elementary matrices $\mathbf{M}_{\theta}^{m}$ as it is proposed by Paggi and Carpinteri (2008). The matrix **A** for the case of a sharp material inclusion (bonded bi-material junction) has the following form:

$$\mathbf{A} = \begin{bmatrix} \mathbf{M}_{\gamma_1}^{0} & -\mathbf{M}_{\gamma_1}^{1} \\ -\mathbf{M}_{\gamma_0=-\frac{\alpha}{2}}^{0} & \mathbf{M}_{\gamma_2=2\pi-\frac{\alpha}{2}}^{1} \end{bmatrix} \tag{14}$$

and the 4×4 elementary matrix $\mathbf{M}_{\theta}^{m}$is

$$\mathbf{M}_{\theta}^{m} = \begin{bmatrix} \frac{\lambda e^{i\theta(\lambda+1)}}{2} & \frac{\lambda e^{-i\theta(\lambda+1)}}{2} & \frac{\lambda(\lambda+1)e^{i\theta(\lambda-1)}}{2} & \frac{\lambda(\lambda+1)e^{-i\theta(\lambda-1)}}{2} \\ \frac{\lambda e^{i\theta(\lambda+1)}}{2i} & -\frac{\lambda e^{-i\theta(\lambda+1)}}{2i} & \frac{\lambda(\lambda-1)e^{i\theta(\lambda-1)}}{2i} & -\frac{\lambda(\lambda-1)e^{-i\theta(\lambda-1)}}{2i} \\ -\frac{e^{i\theta(\lambda+1)}}{4G_m} & -\frac{e^{-i\theta(\lambda+1)}}{4G_m} & \frac{(\kappa_m-\lambda)e^{i\theta(\lambda-1)}}{4G_m} & \frac{(\kappa_m-\lambda)e^{-i\theta(\lambda-1)}}{4G_m} \\ \frac{e^{i\theta(\lambda+1)}}{4iG_m} & -\frac{e^{i\theta(\lambda+1)}}{4iG_m} & \frac{(\kappa_i+\lambda)e^{i\theta(\lambda-1)}}{4iG_m} & \frac{(\kappa_i+\lambda)e^{-i\theta(\lambda-1)}}{4iG_m} \end{bmatrix} \tag{15}$$

A necessary condition for a nontrivial solution of the system of equations (13) to exist is that $\det(\mathbf{A}) = 0$. Development of a matrix determinant leads to a characteristic polynomial equation, whose roots are the eigenvalues λ_k. This polynomial function is in its nature transcendental, thus only a solution by means of numerical methods is admissible. To determine eigenvectors $v_{km} = (M_{km}, \bar{N}_{km}, I_{km}, \bar{L}_{km})$, the kth eigenvalue $\lambda_k$is inserted back into the system of equations (13). Since the system of equations is now undetermined, one of the complex coefficients of the eigenvector v_k is chosen equal to 1. To obtain a determined system of equations, the row and line in the matrix **A** containing the complex coefficient equal to 1 are omitted and a reduced matrix is formed. Based on the solution of this reduced matrix, ratios between complex coefficients are obtained and the eigenvector v_k for each kth λ_k is constructed.

2.4. Determination of Generalized Stress Intensity Factors

The GSIFs H_k are calculated by means of the over-deterministic method as in Ayatollahi and Nejati (2011). No exact solution exists for an over-determined system of linear equations, as is the system (17) below, written in short notation as $\boldsymbol{F}_{[2n\times k]}H_{[k]} = u_{[n]}^{\mathrm{FEA}}$, where $2n > k$. The subscripts describe the dimensions of the matrix or vector. The solution of an over-determined system of linear equations can only be found by minimizing the residual vector $r = \boldsymbol{F}_{[2n\times k]}H_{[k]} - u_{[n]}^{\mathrm{FEA}}$ in some sense, e.g. by the least squares method. The radial and tangential displacement components are in the form

$$u_i = H_1 r^{\lambda_1} f_{i1m}(\theta) + H_2 r^{\lambda_2} f_{i2m} + H_3 r^{\lambda_3} f_{i3m}(\theta) + \dots \tag{16}$$

Both radial and tangential displacement components are used to determine *m* GSIFs. Both the rows of the matrix on the left-hand side and the rows of the vector on the right-hand side are composed of subsequent radial and tangential displacement values of the diameter r and the particular angular coordinate θ_n. The left-hand side represents an analytical solution. The vector on the right-hand side consists of FEA results.

$$\begin{bmatrix} f_{r1}(\theta_1) r^{\lambda_1} & f_{r2}(\theta_1) r^{\lambda_2} & \dots & f_{rk}(\theta_1) r^{\lambda_k} \\ f_{r1}(\theta_2) r^{\lambda_1} & f_{r2}(\theta_2) r^{\lambda_2} & \dots & f_{rk}(\theta_2) r^{\lambda_k} \\ \vdots & \vdots & & \vdots \\ f_{r1}(\theta_n) r^{\lambda_1} & f_{r2}(\theta_n) r^{\lambda_2} & \dots & f_{rk}(\theta_n) r^{\lambda_k} \\ f_{\theta1}(\theta_1) r^{\lambda_1} & f_{\theta2}(\theta_1) r^{\lambda_2} & \dots & f_{\theta k}(\theta_1) r^{\lambda_k} \\ f_{\theta1}(\theta_2) r^{\lambda_1} & f_{\theta2}(\theta_2) r^{\lambda_2} & \dots & f_{\theta k}(\theta_2) r^{\lambda_k} \\ \vdots & \vdots & & \vdots \\ f_{\theta1}(\theta_n) r^{\lambda_1} & f_{\theta2}(\theta_n) r^{\lambda_2} & \dots & f_{\theta k}(\theta_n) r^{\lambda_k} \end{bmatrix} \begin{bmatrix} H_1 \\ H_2 \\ \vdots \\ H_k \end{bmatrix} = \begin{bmatrix} u_{r1}^{\mathrm{FEA}}(r,\theta_1) \\ u_{r2}^{\mathrm{FEA}}(r,\theta_2) \\ \vdots \\ u_{rn}^{\mathrm{FEA}}(r,\theta_n) \\ u_{\theta1}^{\mathrm{FEA}}(r,\theta_1) \\ u_{\theta2}^{\mathrm{FEA}}(r,\theta_2) \\ \vdots \\ u_{\theta n}^{\mathrm{FEA}}(r,\theta_n) \end{bmatrix} \tag{17}$$

3. Numerical Example

The finite element model of a sharp material inclusion was created as shown in Fig. 2. The model is constrained in the *y* direction on the bottom edge and in the bottom left-hand corner point in both the *x* and *y* directions. Then, it is loaded with unit tension denoted σ_∞. The nodal displacements in the radial and tangential directions which serve as an input to the ODM are extracted from the radius surrounding the singular point denoted r_1, the radius is chosen at a distance of 1 mm. The material configurations as listed in Table 1 were examined. Young's moduli of cement paste vary from 25 to 45 GPa, thus configurations of composites with both of these limit values were evaluated. The least stiff cement paste is denoted as cement paste A, the cement paste with the highest stiffness is marked with B. The geometry $\alpha = 80°$ was chosen as a representative for calculated values in Table 1 of this numerical example, although geometries with different angular values were also examined in the study. Plane strain is considered.

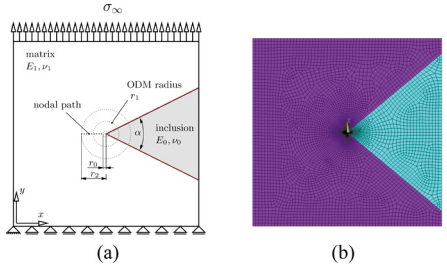

Fig. 2. (a) FE model geometry with a depicted nodal path, (b) FE model mesh illustration.

Table 1 summarizes calculated values of the first 5 singular and non-singular exponents together with corresponding GSIFs values H_k [MPa·m$^{(1-\lambda_k)}$]. In the studied cases there are 2 singular exponents for bi-material configurations with a matrix stiffer than an inclusion (1st and 2nd case) and 1 singular exponent for configurations with a matrix more

compliant than an inclusion (3rd to 6th case). Generally, the configurations with $E_0>E_1$ and with 2 singular exponents can also be found. The polar plots which show the distribution of $\sigma_{\theta\theta}$ in a circular area of 3 mm from the singular point (the radius 0.05 mm surrounding the singular point is intentionally not included) are shown in Fig. 3 and Fig. 4. Each of these figures shows $\sigma_{\theta\theta}$ distribution obtained by (a) singular terms, (b) singular and non-singular terms, (c) FEA. The radius size has been chosen up to 3 mm, since the modelling of fracture processes in silicate / cement based composites requires precise knowledge of stress distribution up to such distances. Since tangential stress can be used for stability criterion suggestion, this numerical example shows this particular stress component.

Table 1. Material properties of matrix / aggregate with calculated values of singular and non-singular exponents and corresponding GSIFs.

Aggregate / Matrix	Young's moduli [GPa]	λ_0	λ_1	λ_2	λ_3	λ_4 [-]
	Poisson's ratios [-]	H_0	H_1	H_2	H_3	H_4 [MPa·m$^{(1-\lambda k)}$]
Sandstone / Cement paste A	20 / 25	0.96816	0.99116	1.03887	1.94338	1.975514
	0.20 / 0.20	0.170646	0.00015	-0.023723	0.000049	0.000153
Sandstone / Cement paste B	20 / 45	0.87363	0.96004	1.14793	1.82212	1.904488
	0.20 / 0.20	0.277678	0.000496	-0.023358	0.00098	0.000671
Granite / Cement paste A	50 / 25	0.89110	1.00582	1.08128	1.865566 - 0.032483i	1.865566 + 0.032483i
	0.24 / 0.20	-0.022447	-0.003085	0.109534	0.000479	0.000256
Granite / Cement paste B	50 / 45	0.98013	1.00223	1.01728	1.985947 - 0.010532i	1.985947 + 0.010532i
	0.24 / 0.20	0.011091	-0.001042	0.106946	0.000515	0.000447
Basalt / Cement paste A	60 / 25	0.86740	1.00020	1.09657	1.829640 - 0.017765i	1.829640 + 0.017765i
	0.25 / 0.20	-0.024563	-0.135623	0.105457	0.000357	0.000427
Basalt / Cement paste B	60 / 45	0.94876	1.00608	1.04182	1.950470 - 0.025195i	1.950470 + 0.025195i
	0.25 / 0.20	-0.005806	-0.000868	0.112457	0.000423	0.000269

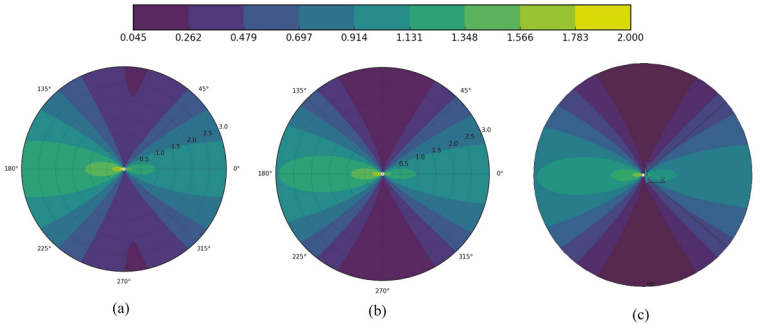

Fig. 3: A reconstructed 2D tangential stress field of Aggregate / Matrix configuration of Sandstone / Cement paste B by: (a) singular terms only; (b) singular and non-singular terms; (c) FEA solution

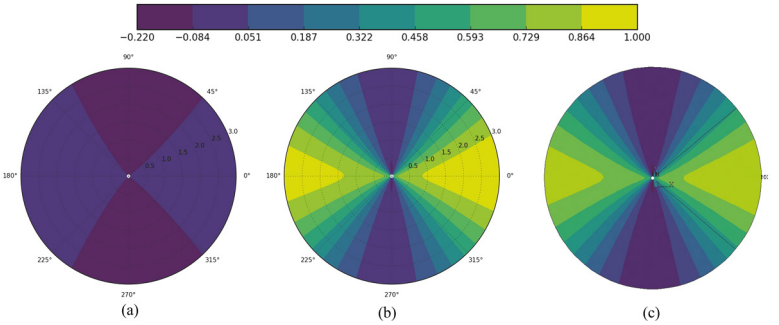

Fig. 4: A reconstructed 2D tangential stress field of Aggregate / Matrix configuration of Basalt / Cement paste A by (a) singular term only; (b) singular and non-singular terms; (c) FEA solution

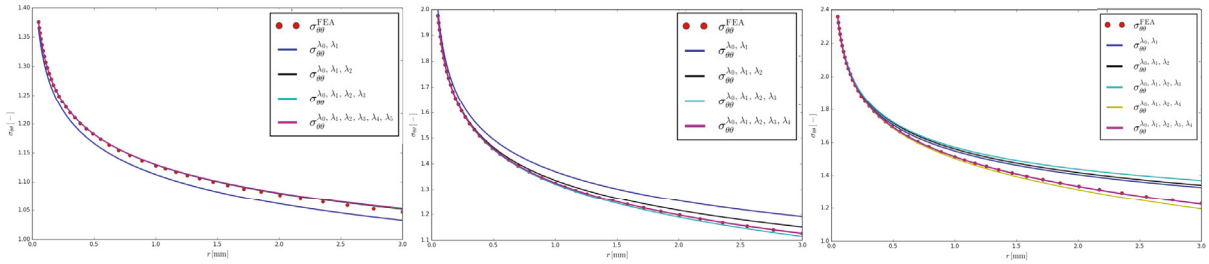

(a) (b) (c)

Fig. 5: $\sigma_{\theta\theta}$ on a path for a bi-material combination of Sandstone / Cement paste B, configurations: (a) $\alpha = 40°$; (b) $\alpha = 80°$; (c) $\alpha = 120°$

It is evident that for E_0<E_1 (Fig. 3) a singular terms solution is close to an FEA solution, while for E_0<E_1 (Fig. 4) both singular and non-singular stress terms are necessary to describe stress distribution precisely. Fig. 5 shows the distribution of $\sigma_{\theta\theta}$ on a straight path, originating near the singular point (0.05 mm) and terminating at a 3 mm distance from the inclusion tip, for various geometric configurations. The graphs show $\sigma_{\theta\theta}$ determined by singular and non-singular terms in comparison with the FEA results. The path location is illustrated in Fig. 2a. Note that for the increasing angle α the effect of higher terms on precision of the stress description becomes more significant. As it can be noted from the polar plots in Fig. 3 and Fig. 4, the choice of an angle under which the path is constructed may lead to even higher differences in stress obtained by singular terms in comparison with either a singular or non-singular terms solution or FEA.

4. Conclusions

It has been found that for geometric and material configurations of sharp material inclusions where an inclusion is more compliant than a matrix, accounting for the non-singular terms of the series leads to more precise results further away from the singular point. The higher opening angle of the inclusion also makes employment of higher order terms more critical for description precision. For the geometric and material configurations of SMI where the inclusion is stiffer than matrix, the stress description by only 1 or 2 singular terms is not sufficient and leads to misleading results.

Acknowledgements

This research has been financially supported by the Ministry of Education, Youth and Sports of the Czech Republic under the project CEITEC 2020 (LQ1601). The authors would like to thank the Czech Science Foundation for financial support through the Grant 16/18702S.

References

Williams, M. L., Pasadena, C., 1957. On the Stress Distribution at the Base of a Stationary Crack, Journal of Applied Mechanics 24, 109-114

Williams, M. L., Pasadena, C., 1952. Stress Singularities Resulting From Various Boundary Conditions in Angular Corners of Plates in Extension, Journal of Applied Mechanics 19, 526-528.

Muskhelishvili, N. I., 1953. Some basic problems of the mathematical theory of elasticity, trans. by I. R. M. Radok, Noordhoff, Groningen.

England, A. H., 2003. Complex Variable Methods in Elasticity, Donver Pub., New York.

Paggi, M., Carpinteri, A., 2008. On the Stress Singularities at Multimaterial Interfaces and Related Analogies With Fluid Dynamics and Diffusion, Applied Mechanics Reviews 61.

Hein, V. L., Erdogan, F., 1971. Stress Singularities in a Two-Material Wedge, International Journal of Fracture Mechanics 7, 317-330

Pageau, S. S., Joseph, P. F., Biggers, S. B. Jr., 1994. The Order of Stress Singularities for Bonded and Disbonded Three Material Junctions, Int.J. Sol. Struct., 31, 2979-2997.

Yang, Y. Y., Munz, D, 1995. Stress Intensity Factor and Stress Distribution in a Joint with an Interface Corner under Thermal and Mechanical Loading, Computers & Structures, 57, 467-476

Sator, C., Becker, W., 1991. On stress singularities at plane bi- and tri-material Junctions – A way to derive some closed form analytical solutions, Procedia Engineering 10, 141-146

Theocaris, P. S., 1974. International Journal of Engineering Science 12, 107-120

Ayatollahi, M.R., Nejati, M., 2011. International Journal of Mechanical Sciences 53. 164–177